5-12-2019

High-Torque-Density Low-Cost Magnetic Gear Utilizing Hybrid Magnets and Advanced Materials

Ali Hussain Al-Qarni
Marquette University

Fan Wu
Marquette University

Ayman M. EL-Refaie
Marquette University, ayman.el-refaie@marquette.edu

2019 IEEE International Electric Machines & Drives Conference (IEMDC), (May 12, 2019): 225-232. DOI.

High-Torque-Density Low-Cost Magnetic Gear Utilizing Hybrid Magnets and Advanced Materials

Ali Al-Qarni
Department of Electrical and Computer Engineering, Marquette University, Milwaukee
Fan Wu
Department of Electrical and Computer Engineering, Marquette University, Milwaukee
Ayman El-Refaie
Department of Electrical and Computer Engineering, Marquette University, Milwaukee

Abstract:

Two major challenges of existing high-performance magnetic gears are: (i) High content of rare-earth permanent magnets which results in high cost as well as price fluctuation; (ii) Conflict between mechanical and electromagnetic performances, especially in the design of highspeed rotor. A magnetic gear using a blend of magnet types, i.e NdFeB, or Dy-free NdFeB and ferrites, is proposed in this paper. The goal is to bring down the cost while retaining comparable torque-transducing performance to a baseline magnetic gear only using rare-

earth NdFeB magnets. A variety of topologies based on different combinations of magnet types and geometric shapes have been studied and compared. In addition, the potential impact of using an advanced dual-phase material is evaluated. The goal is to eliminate the well-known tradeoff between rotor mechanical integrity and PM flux leakage.

SECTION I. Introduction

The ability to scale the torque/speed enables designing electrical machines for higher speeds/lower torques and hence reduce their size and cost. Such ability is accomplished by using gearboxes. Gearboxes are used in a wide range of applications including renewable energy, aerospace and traction applications among others. In addition to the size/cost reduction of electrical machines, gearboxes are needed in some applications for example traction where driving a vehicle requires multi gear ratios to match the load torque/speed requirements. Mmechanical gearboxes have historically dominated most applications. However, they suffer from tooth breakage, periodic maintenance, and less reliability. On the other hand, coaxial magnetic gears (MGs), as shown in Fig. 1, is a promising candidate to replace mechanical gears in some applications since they fundamentally function in the same way but with the advantage of physical isolation between the shafts. This unique feature offers overload protection, higher reliability, and less noise operation [1]. Coaxial MG working principle is well known and is based on the interaction of the harmonic frequency components produced by one rotor in its adjacent airgap and after being modulated by the flux modulation pole-pieces (FMP-Ps) in the non-adjacent airgap to coincide with the other rotor harmonic frequency components and then a useful torque transmission can be transduced. The expression governing the flux modulation concept is given by (1).

$$\begin{aligned} f_{mk} &= |mP + kN_s| \\ m &= 1,3,5,7,9,\dots\dots,\infty \\ k &= 0,\pm1,\pm2,\pm3,\dots,\pm\infty \\ N_s &= P_{LSR} + P_{HSR} \end{aligned} \qquad (1)\ (2)$$

where P is the number of pole pairs; Ns is the number of FMP-Ps, and fm, k is the harmonic frequency. When $(m = 1 \& k = -1)$, this corresponds to the useful flux modulation and torque transducing case. There are some other super and sub harmonics that do not contribute to torque transducing but tend to generate iron losses and torque ripple. For better torque transmission, the number of FMP-Ps should equal the sum of the pole-pairs of the low-speed rotor (LSR) and highspeed rotor (HSR) as indicated in (2). Moreover, since all the three rotors are able to rotate, we can have three different gear ratios by making one of them stationary and let the other two rotors rotate as shown in (3),

$$G_{r_1} = \frac{P_{LSR}}{P_{HSR}}, G_{r_2} = \frac{N_S}{P_{HSR}}, or G_{r_3} = \frac{N_S}{P_{LSR}} \quad (3)$$

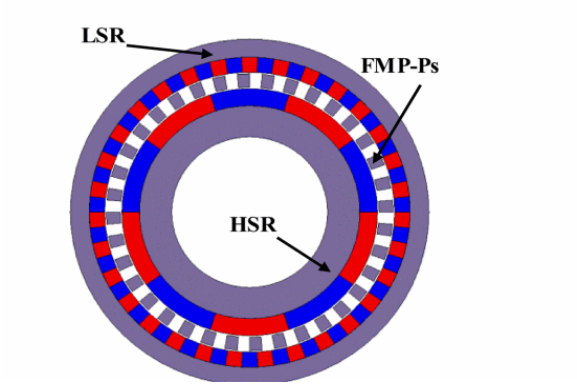

Fig. 1. Surface mounted coaxial MG with gear ratio of 7.2

The torque equation assuming no loss operation is given by (4):

$$T_{FMP-Ps} + T_{LSR} + T_{HSR} = 0 \quad (4)$$

Alternatively, controlling the speed of one rotor enables continuously variable transmission [2].

Although MG can potentially provide a solution for some of the practical issues of mechanical gears, MGs have their own challenges that researchers are trying to address. Those include relatively limited tip speed on HSR [3]–[4][5], low torque density [4]–[5][6][7][8][9][10][11], complexity in structure [12]–[13][14][15][16][17], as well as the significant use of rare-earth permanent magnets (PMs) [16]–[17][18]. In addition, like in conventional electrical machines, there are several design tradeoffs involved. For example, [3] demonstrates a MG prototype with the highest torque density reported in literature so far [19], [20]. However, the rotor tip speed is limited by the segmented structure. In [7], although a HSR with interior PMs and FMP-Ps with two supportive bridges were adopted to improve their mechanical strength, torque density was significantly reduced.

Since the shear stress in a MG is only constrained by the magnetic loading, large quantities of PMs are typically used to maintain high shear stress level. Therefore, the objective of this paper is to design a spoke-PM HSR with a blend of different magnets. This results in minimization of the overall materials cost while achieving comparable torques production to a baseline design that only uses rare-earth PMs. It will be shown that by using this hybrid approach, ~36% reduction in HSR rare-earth PM usage can be achieved with only 6% or lower reduction in torque production. Moreover, the use of dual-phase material in the HSR rotor as well as a dovetailed HSR are discussed. Both concepts can maintain mechanical integrity of the HSR when spinning at high tip speeds while minimizing/eliminating PM leakage flux. For the LSR, the PMs are embedded in cavities to enhance the mechanical structure while the trapezoid FMP-Ps use laminated steel sheets with high yield strength.

This paper is arranged as follows: the design parameters and corresponding analyses are included in Section II. Section III discusses the feasible combinations with a blend of different magnet types and a down-selection process of the optimum combination is discussed. Section III also provides a comparison of different potential geometries of the HSR. Section IV investigates methods to improve the structural integrity of the HSR while minimizing/eliminating PM flux leakage then conclusions.

SECTION II. Design Anaysis and Details

A. Topology and Gear Ratio

A comparative study between various rotor designs targeting at high torque density was presented in [21]. MGs using spoke PMs are well-known for their high torque density due to flux concentration effect, as shown in Fig. 2. Moreover, in order to reduce the size and cost of a MG, a high gear ratio is always preferred. However, there are still some challenges for further increasing the torque density. In [22], a comprehensive study on the parameters that affect the torque capability proves that as the gear ratio increases, the torque capacity on the FMP-Ps gets lower. Moreover, one of these parameters that is correlated with the high gear ratio is the reduced width of the LSR PMs in which might result in impractical PM shapes from a manufacturing point of view as well as reduced airgap flux density due to the increased flux leakage. The torque ripple of a MG, which is associated with the least common multiple (LCM) of the HSR pole-pair and FMP-Ps for stationary LSR operation, is fairly low with high gear ratio. A study on the gear ratio selection for the listed combinations in Table I was performed to identify a compromise between the aforementioned challenges and the following considerations. It should be noted that integer gear ratios are avoided since they tend to have low LCM (PHSR,Ns)compared to fractional

gear ratios [23]. Also. it is recommended to choose an even number of Ns in order to have symmetrical radial forces that would cancel out. The gear ratio for stationary LSR operation and the LCM between (PHSR,Ns) are both shown in Table I. Since the proposed topology is designed to run at high tip speed, a constraint on the HSR radius is required. A design tradeoff can be shown here, since the HSR rotor radius is constrained at 95 mm. High pole-pair number minimizes the space to employ low remanence magnet (LRM). On the other hand, a low pole-pair number in the HSR leads to a larger pole span which becomes challenging to retain when the rotor is equipped with LRM. Table I demonstrates that the LCM is fairly high for all combinations. However, at this HSR outer radius the combination listed in Table IIleads to a LSR pole thickness of 5 mm assuming at least 8 mm FMP-Ps radial thickness. The HSR pole-pair for this combination provides enough space for LRM. The MG specifications are listed in Table II.

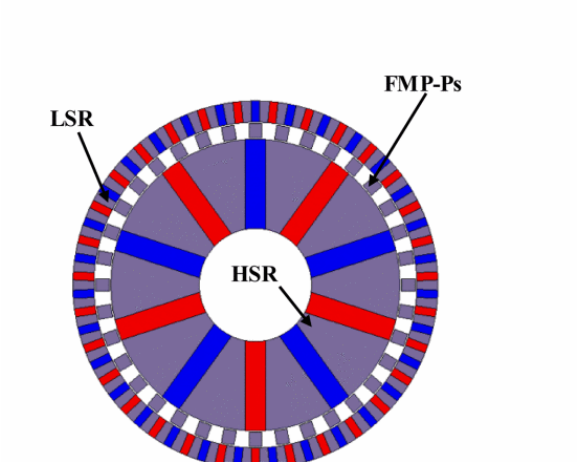

Fig. 2. Spoke coaxial MG with gear ratio of 7.2

Table I. Gear ratio combinations

P_{HSR}	P_{LSR}	N_s	G_r	LCM (P_{HSR}, N_s)
4	25	29	7.25	116
4	27	31	7.75	124
5	31	36	7.2	180
5	32	37	7.4	185
5	33	38	7.6	190
5	34	39	7.8	195
6	37	43	7.16	258
6	38	44	7.33	132
6	40	46	7.66	138
6	41	47	7.83	282

Table II. Model specifications

Parameter	Value & Unit
HSR Pole-Pair (rotational)	5
LSR Pole-Pair (fixed)	31
FMP-Ps (rotational)	36
Gear ratio	7.2

B. Choice of Materials

In MGs, the magnetic loading is the only source of excitation to accomplish high torque per unit volume. This gives rise to higher usage of rare-earth PM materials as can be seen in the spoke design. Blending different PM types can be an effective solution that can mitigate this penalty while having comparable torque density. The proposed topology has a blend of rare-earth PMs (either Dy-NdFeB or Dy-free NdFeB) with Ferrites. The Dy-free NdFeB has higher remanence compared to the Dy-NdFeB as shown in Table III. The proposed MG can be potentially designed to have a high- tip-speed HSR in which a relatively high-yield-strength material is required for reliable operation with variable loads and physical environments. HF-10 from AK Steel (with yield strength of 450 MPa) is adopted in the design. Material specifications are listed in Table III with assumptions of their market prices. It should be noted that material prices are influenced by the market supply/demand as well as quantities of purchase.

Table III. Summary of materials and prices

Material Type	Material Commercial Name/ Price
Lamination	DI-MAX HF-10 by AK Steel (10 mils or 0.25 mm thickness) [2 $/kg] [7600 kg / m^3]
NdFeB-Dy PM	Arnold N40H (B_r = 1.25 T) (μ_r= 1.07 H/m) [100 $/kg] [7500 kg/$m^3$]
NdFeB-Dy free PM	Vacuumschelze VACODYM 238TP (Br = 1.33 T) (μ_r = 1.05 H/m) [60 $/kg] [7600 kg/$m^3$]
Ferrite PM	Ferrite NMF-12G (Br = 0.48 T) (μ_r = 1.06 H/m) [10 $/kg] [4800 kg/$m^3$]
Shaft	Non-magnetic 304 Stainless Steel [4 $/kg] [8190 kg/$m^3$]

C. Optimization of Baseline Design

An optimization tool has been coupled with 2D-FEA to conduct a multi sweep range of seven independent variables in order to reach an optimum baseline design. A summary of the independent variables and their sweep ranges are summarized in Table IV. The key parametric model corresponding to Table IV is shown in Fig. 3. The outer radius of the HSR is kept constant, which has a significant impact on determining the general design geometries. The FMP-Ps radial thickness is given by (5):

$$R_3 = R_2 + a + x_1 \quad (5)$$

The outer MG radius is given by (6):

$$R_4 = R_2 + 2 * a + x_1 + w_1 \quad (6)$$

The magnet inner arc length in the LSR is kept equal to the neighboring iron piece and has a rectangular shape. In Fig. 4, a map of designs was generated by using 2D-FEA showing the torque density versus the specific torque. The torque density calculation is given by (7):

$$TD = \frac{T_{FMP-Ps}}{\pi * R_4^2 * L} \quad (7)$$

The specific torque is calculated by (8):

$$ST = \frac{T_{FMP-Ps}}{mass} \quad (8)$$

where the mass is calculated based on each material volume multiplied by the corresponding density listed in Table III. The optimal design variables, that achieves the highest torque density, are listed in Table IV while, the average torque density and specific torque values of the optimal design are listed in Table V.

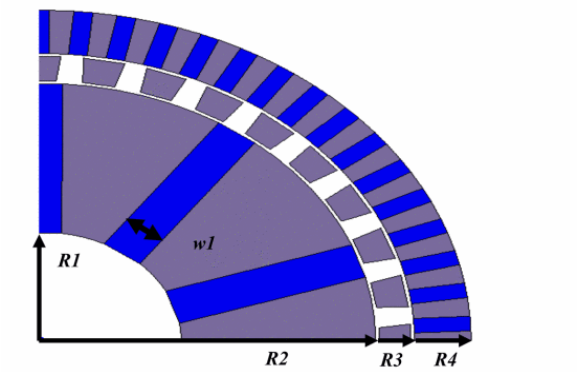

Fig. 3. Baseline key parameter model.

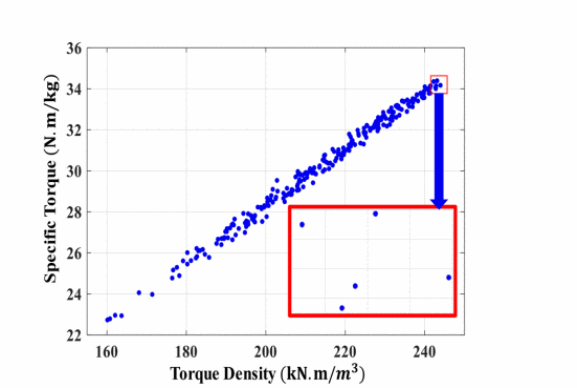

Fig. 4. Map of designs showing the torque density vs. Specific torque.

Table IV: Geometries sweep range

Parameter	Sweep Range	Step	Optimal Design	Unit
FMP-Ps Radial Thickness, (x1)	8-12	0.5	9	(mm)
HSR Inner Radius, (R1)	40-60	1	40	(mm)
HSR Outer Radius, (R2)	Fixed	-	95	(mm)
Airgap Thickness, (a)	Fixed	-	1	(mm)
LSR Radial Thickness, (x2)	10-17	1	16	(mm)
Inner FMP-Ps Angular Span, (γ)	5-7	0.5	5.5	(deg)
Outer FMP-Ps Angular Span, (β)	5-7	0.5	6.5	(deg)
Axial Length, (L)	70-90	2	86	(mm)
HSR PM Width, (w1)	10-13	0.5	12.5	(mm)

Table V: Baseline torque capability

Parameter	Value	Unit
Torque	980	(N.m)
Torque Density	243.7	(kN. m/m^3)
Specific Torque	34.4	(N. m/kg)

SECTION III. Designs with Different Magnet Types

A. Geometric Anaylsis

This section covers the utilization of different magnet types in five designs. It should be noted that all design variables are kept fixed except the PM thickness in the HSR and the inner HSR radius to enable LRM adoption. First, the baseline design is simulated using Dy-NdFeB. Then, the other two types of magnets (Dy-free NdFeB and

Ferrite) were used to check the torque capability when using each of them separately. For designs 4 and 5, a rectangular parallel hybrid PMs consist of three layers were modeled using a parametrized model for the PM thickness to achieve the highest torque. The ferrite is sandwiched in between the rare-earth NdFeB layers. Design 4 uses a blend of NH40 (Dy-NdFeB) and NMF-12G (Ferrite), whereas design 5 adopts VACODYM 238TP (Dy-free NdFeB) and NMF-12G (Ferrite). The HSR inner radius became 44 mm to provide space for the LRM adoption. This leads to ~36% reduction of rare-earth PM volume used in the HSR while the overall rare-earth magnet is reduced by ~21% Also, ~27% increase in the overall HSR PM volume compared to the first two designs due to the higher volume of ferrite. In terms of the mass of PMs, the reduction of the overall rare-earth magnet mass for designs 4 and 5 is almost 21 %, compared to designs 1 and design 2. Table VI shows the overall changes in the model geometries. This development leads to a marginal difference in the torque capability for the proposed designs as will be shown next.

B. FEA Results and Comparison Between Toplogies

In this section, the performances of design 1 and 2 are compared to designs 4 and 5. The following results are obtained using static 2D-FEA simulation. The models and flux distribution are shown in Fig. 5. The flux density level in the HSR lamination is relatively low around 1.5 T while the flux density level in the FMP-Ps is about 1.7 T. It can be seen from Fig. 5 that the end effect leakage (fringing) is significant and can have a relatively significant impact on the transferred torque. The radial space harmonic plots for both airgaps with corresponding harmonic spectra are provided in Figs. (6)and (7). The dominant harmonics for torque transducing are the ones with 5 and 31 pole-pairs respectively. There are some other harmonics in the inner airgaps when (m>1 & k=0) in (1), specifically, the ones with 15,25, and 35 pole-pairs. These harmonics do not couple with any in the outer airgap when they are modulated (m>1 & k≠0) in (1). For the outer airgap, the main torque producing harmonic is the one with 31 pole-pairs. In Table VII, the torque on the various components (HSR, LSR, FMP-Ps) for the five designs agrees with (4). Design 2 has the highest torque density due to the higher remanence of the Dy-free PM, while design 1 is lower by ~4percent. It is shown from Table VII that the variance in the torque density between designs 4 and 5 is about 3.6%. Furthermore, the achievable torque density in designs 4 and 5 is lower compared to designs 1 and 2 by ~6%, However, the specific torque for designs 4 and 5 are maintained at the same level as designs 1 and 2 by the virtue of lower density of ferrite.

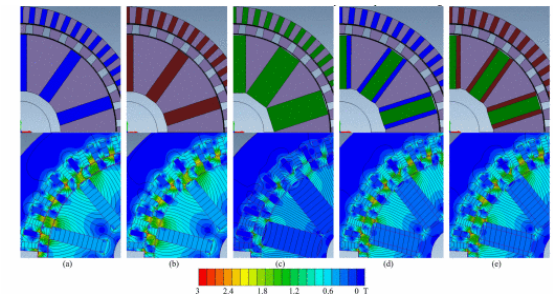

Fig. 5. Design solid model with the corresponding field plot (NdFeB-DY is in blue color. Ndfeb-dy-free is in brown color, while the green is ferrite): (a) Design 1, (b) design 2, (c) design 3, (d) design 4, (e) design 5

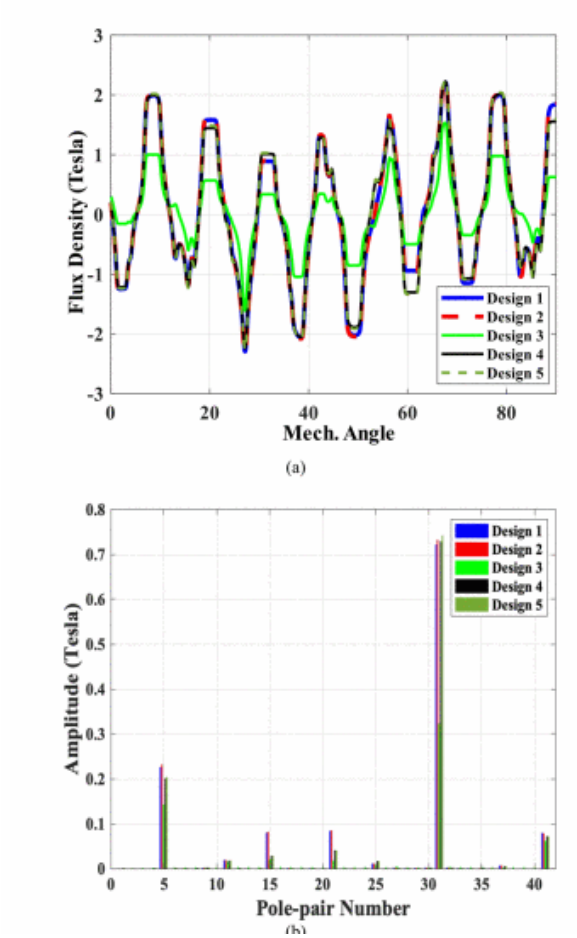

Fig. 6. Outer airgap flux density with its harmonic spectra.

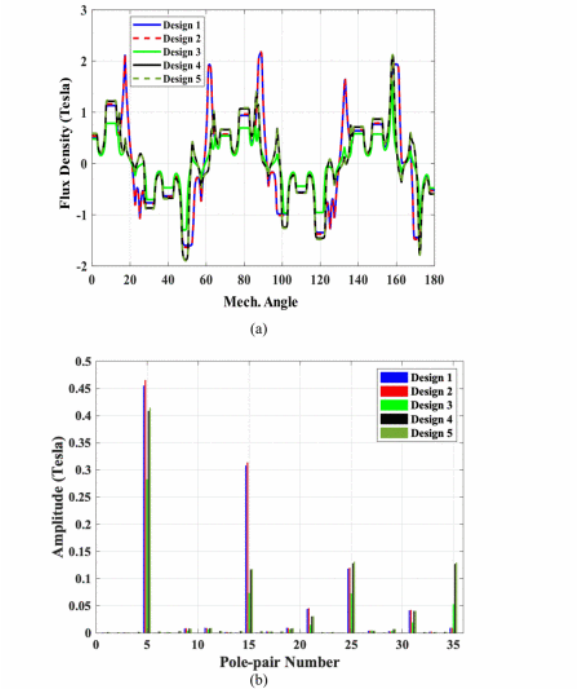

Fig. 7. Inner airgap flux density with its harmonic spectra.

Table VI: Geometries change

Design Number	PM Width (mm)		HSR PM Mass (kg)	

	Rare-earth	LRM	Rare-earth	LRM
Design 1 Dy-NdFeB	12.5	--	4.45	--
Design 2 Dy-free NdFeB	12.5	--	4.5	--
Design 3 Ferrite	--	24.4	--	5.531
Design 4 Dy-NdFeB and Ferrite	8.5	13.45	2.85	2.9
Design 5 Dy-free NdFeB and Ferrite	8.5	13.45	2.9	2.9

Table VII: Torque capability of different designs

Design Number	Torque on Components (N. m)			Torque Density (kN. m/m^3)	Specific Torque (N. m/kg)
	HSR	LSR	FMP-Ps		
Design 1	-136	-844	980	243.7	34.4
Design 2	-142	-878	1020	253.6	35.7
Design 3	-35	-217	252	62.6	10.5
Design 4	-128	-794	922	229.3	34.4
Design 5	-133	-823	956	237.7	35.6

C. Possible Hybrid Magnet Designs

So far, the focus has been a parallel-sided PM geometry. In this section, other geometries will be evaluated all of which has the same ration of NdFeB to ferrite as in design 4 from the previous section. The considered designs and their corresponding flux plots are shown in Fig. 8 and obtained using static 2D-FEA simulation. As can be seen in Figs. 8(a) and (b), the use of trapezoidal magnets results in significant leakage flux near the rotor inner surface, which is inefficient for torque transmission in comparison to rectangular PMs. This is due to the flux leakage path through the shaft. Additionally, it is hard to retain the pole with larger span in order to come up with comparable performance to the baseline design. The series magnet combination can produce a comparable torque density to the parallel design case (Figs. 8(c) and (d)). However, the utilization of LRM in this case is fairly low since ferrite behaves as a flux barrier and intensifies the flux along the flux path generated by rare-earth magnets. This results in little interaction between LRMs with rare-earth magnets due to the fact that the operating points of the rare-earth magnets and LRMs are different.

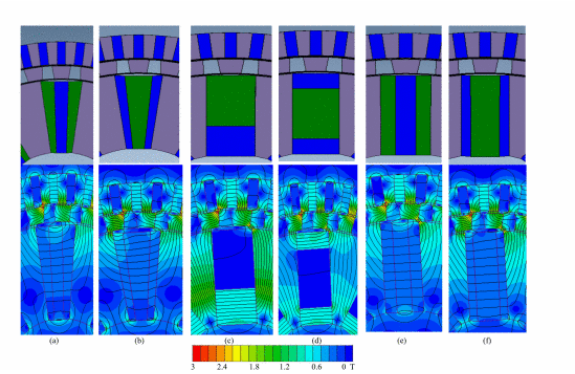

Fig. 8. Different hybrid magnet combination with the corresponding field plot and torque performance (NdFEb-DY is in blue color, while the green is ferrite): (a) Trapezoid shape 1, (b) Trapezoid shape 2, (c) Series shape 1, (d) Series shape 2, (e) Parallel shape 1, (f) Parallel shape 2

The parallel combination can produce comparable transferred torque because the flux is uniformly distributed in the lamination with less leakage inward the shaft. A better performance for the parallel combination can be achieved if the LRM is sandwiched between the NdFeB layers as shown in Fig. 8(f). This results in stronger field

in the HSR core compared to case (e). Table VIII shows the torque performance for the six different combinations. It can be concluded that the design with the ferrite sandwiched between the NdFeB magnets is the optimum combination.

Table VIII: Torque capability of different hybrid combinations

Case Magnet Shape Torque (N.m)		
(a) Trapezoid shape	1	800
(b) Trapezoid shape	2	878
(c) Series shape	1	895.5
(d) Series shape	2	893
(e) Parallel shape	1	850
(f) Parallel shape	2	922

D. Cost Analysis

The feasibility of the reduced rare-earth topologies was shown in terms of performance. It will be seen that in terms of cost minimization, the proposed topology is even more encouraging. Based on the material prices in Table II, design 1 costs more with lower torque density in comparison to design 2. Clearly, ferrite is the lowest in performance and cost when it is used alone. A cost reduction of ~17 and 14 % can be achieved in designs 4 and 5 respectively compared to designs 1 and 2 as shown in Fig. (9). For the hybrid topologies, design 4 has lower torque capability compared to design 5 with even higher cost (by ~ 54 %).

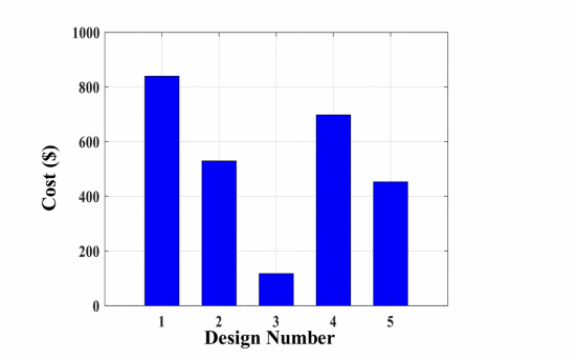

Fig. 9. Materials cost for various designs.

SECTION IV. Mechanical Design Options

In all the previous analysis, it was assumed that there are no bridges in the LSR and HSR. Even though this assumption should not change the relative results, or the trends discussed, this section will cover some potential options to build the rotors either without bridges or with bridges but minimize the PM flux leakage in the bridges.

A. HSR with Dual Phase Material

The mechanical design is critical especially for high tip speeds. Based on the obtained results in the previous section, design 5 is chosen to be the optimum design for further consideration. The first option to be investigated is the adoption of a dual-phase magnetic material for the HSR laminations. Nonmagnetic regions can be selectively introduced in rotor bridges [24]. This will enable increasing the thickness of these bridges to withstand higher mechanical stresses without worrying about the PM flux leakage in these regions. Also, the yield strength of the non-magnetic regions of the dual-phase magnetic material is roughly twice that of the magnetic regions which further help withstand higher mechanical stresses due the high tip speed. Consequently,

design 5 was modeled in 2D-FEA utilizing the dual-phase magnetic material with bridge thickness of thickness 1mm to show the potential of such material. As can be seen, the nonmagnetic bridges lead to minimum leakage flux (Fig. 10(b)) compared to significant leakage in case of a magnetic bridges (Fig. 10(c)). It should be noted also that the torque was reduced by 9% to be 869 N.m when the bridges are magnetic as in (Fig. 10(c)).

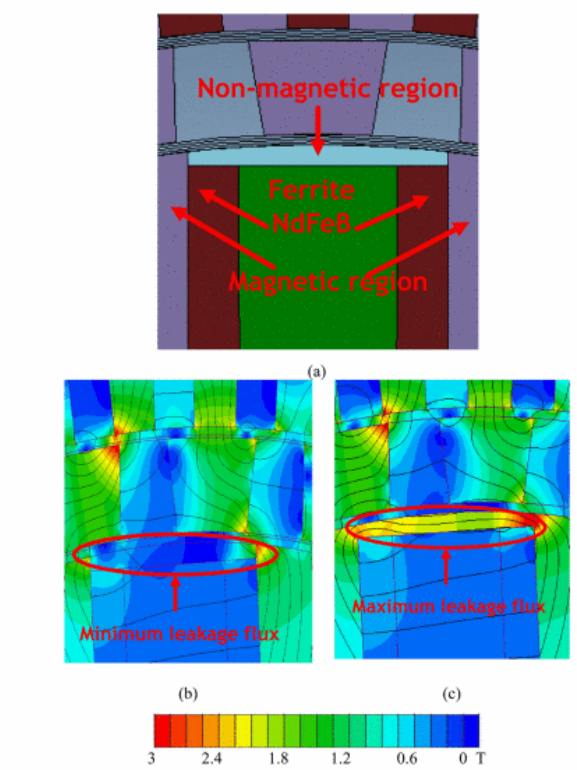

Fig. 10. Dual-phase material design: (a) Indication of the dual-phase material location (b) flux plot with dual-phase material (c) flux plot without the dual-phase material.

B. HSR with Dovtalied Design

Another option is to have the HSR laminations dovetailed to a non-magnetic shaft. A similar dovetailed design was presented in [25]. This dovetailed approach can be implemented alone and lead to a segmented rotor structure with no bridges (as was demonstrated in [25]) or it can be potentially implemented in conjunction with the dual-phase magnetic material as shown in Fig, 11 to further strengthen the HSR. The reduction in torque when implementing the dovetailed shaft was ~26 N.m to be 929.2 N.m. this reduction maight be reduced with further analysis.

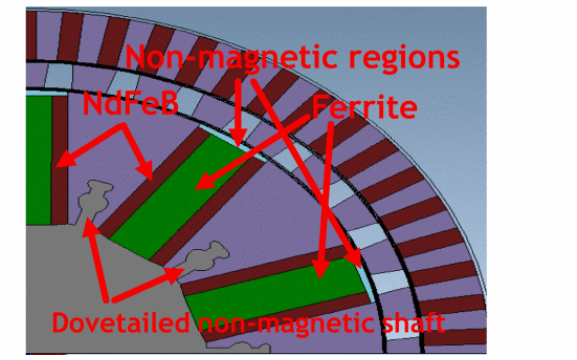

Fig. 11. Potential design with dovetailed shaft and dual-phase material in the HSR.

C. LSR Design

Regarding the LSR, due to the large number of poles, it might be difficult to implement similar options discussed for the HSR. In this case, the simplest solution is to have the PMs buried inside the LSR laminations, effectively creating an IPM rotor. In this case, the bridges will present an electromagnetic penalty as expected. Table IX shows the torque reduction with respect to the bridges thickness. As can be seen, the torque production is very sensitive to the bridge thickness. Since in this study, we have been assuming that the LSR is stationary, a bridge thickness of a 0.5 mm or thinner can be used.

Table IX. Designs torque capability

Bridges Thickness (mm)	Torque (N.m)
0	929.2
0.25	857.1
0.5	781
0.75	714.5

D. Dynamic Torque

Based on 0.5 mm LSR bridge thickness, the average torque of the design is 781 N.m. The final parameters for this optimal design are listed in Table X. The dynamic torque on the FMP-Ps over one electrical cycle is shown in Fig. 12. As can be seen, the peak-to-peak torque ripple on the FMP-Ps is about 3 N.m average which is below 0.3% of the average torque. This is considered fairly low. In addition to the torque production, it is expected that the proposed topology with the blend of magnets will have higher efficiency due to the significantly higher electrical resistivity of ferrite.

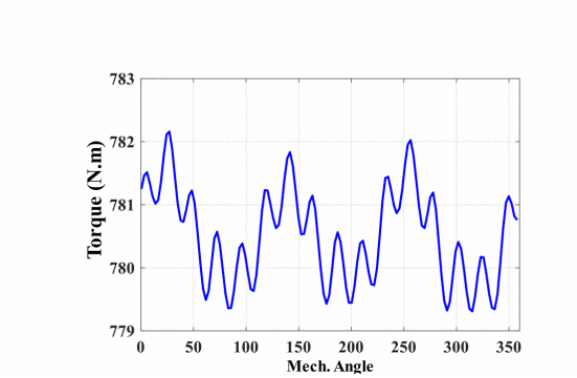

Fig. 12. Dynamic torque on the FMP-Ps.

Table X. Final design parameters

Parameter	Value
HSR Dual-phase bridge thickness (mm)	1
LSR bridge thickness (mm)	0.5
HSR Inner Radius (mm)	46
LSR Outer Radius (mm)	123
Torque Density (kN. m/m_)	191.1
Specific Torque (kg)	29.06

SECTION V. Conclusion

A MG with a blend of NdFeB and ferrite magnet has been proposed. It was shown that the torque density of the proposed topology is ~6% lower the baseline rare-earth design while the specific torque is maintained due to the lower density of ferrites. The material cost is reduced by 21%. In addition, some options to enable high tip speeds in the HSR while minimizing/eliminating PM flux leakage in the bridges have been discussed. In addition to the torque production, it is expected that the proposed topology with the blend of magnets will have higher efficiency due to the significantly higher electrical resistivity of ferrite.

REFERENCES

[1] K. Atallah and D. Howe, "A novel high-performance magnetic gear," IEEE Trans. Magn., vol. 37, no. 4, pp. 2844-2846, 2001.

[2] Z. Q. Zhu, H. Y. Li, R. Deodhar, A. Pride and T. Sasaki, "Recent developments and comparative study of magnetically geared machines," CES Transactions on Electrical Machines and Systems, vol. 2, no. 1, pp. 13-22, March 2018.

[3] K. K. Uppalapati, J. Z. Bird, J. Wright, J. Pitchard, M. Calvin, and W.Williams, "A magnetic gearbox with an active region torque density of 239Nm/L," in Proc. IEEE Energy Conversion Congress and Exposition (ECCE), Sept. 2014, pp. 1422-1428.

[4] K. Atallah, S. D. Calverley, and D. Howe, "Design, analysis and realisation of a high-performance magnetic gear," IEE Proceedings - Electric Power Applications, vol. 151, no. 2, pp. 135-143, 2004.

[5] L. Jian, K. T. Chau, Y. Gong, J. Z. Jiang, C. Yu and W. Li, "Comparison of Coaxial Magnetic Gears With Different Topologies," in IEEE Transactions on Magnetics, vol. 45, no. 10, pp. 4526-4529, Oct. 2009.

[6] P. O. Rasmussen, T. O. Andersen, F. T. Joergensen and O. Nielsen, "Development of a high performance magnetic gear," 38th IAS Annual Meeting on Conference Record of the Industry Applications Conference, 2003., Salt Lake City, UT, USA, 2003, pp. 1696-1702.

[7] N. W. Frank and H. A. Toliyat, "Analysis of the concentric planetary magnetic gear with strengthened stator and interior permanent magnet inner rotor," IEEE Trans. Ind. Appl., vol. 47, no.4, pp. 1652-1660, 2011. [8] X. Liu, K. T. Chau, J. Z. Jiang, and C. Yu, “Design and analysis of interior-magnet outer-rotor concentric magnetic gears,” Journal of Applied Physics, vol. 105, no. 7, p. 07F101, 2009.

[9] K. Aiso and K. Akatsu, “A novel reluctance magnetic gear for high speed motor,” in Proc. IEEE Energy Conversion Congress and Exposition (ECCE), Sept 2016, pp. 1–7.

[10] P. O. Rasmussen, H. H. Mortensen, T. N. Matzen, T. M. Jahns and H. A. Toliyat, "Motor integrated permanent magnet gear with a wide torque-speed range," 2009 IEEE Energy Conversion Congress and Exposition, San Jose, CA, 2009, pp. 1510-1518.

[11] J. J. Scheidler, V. M. Asnani and T. F. Tallerico, "NASA's Magnetic Gearing Research for Electrified Aircraft Propulsion," 2018 AIAA/IEEE Electric Aircraft Technologies Symposium (EATS), Cincinnati, OH, 2018, pp. 1-12.

[12] X. Yin, P. D. Pfister, and Y. Fang, "A novel magnetic gear: toward a higher torque density," IEEE Transactions on Magnetics, vol. 51, no. 11, pp. 1-4, 2015.

[13] S. Peng, W. N. Fu, and S. L. Ho, "A novel triple-permanent-magnet excited hybrid-flux magnetic gear and its design method using 3-D finite element method," IEEE Trans. Magn., vol. 50, no.11, pp. 1-4, 2014.

[14] D. Zhu, F. Yang, Y. Du, F. Xiao and Z. Ling, "An Axial-Field FluxModulated Magnetic Gear," in IEEE Transactions on Applied Superconductivity, vol. 26, no. 4, pp. 1-5, June 2016, Art no. 0604405.

[15] Li Yong, Xing Jingwei, Peng Kerong and Lu Yongping, "Principle and simulation analysis of a novel structure magnetic gear," 2008 International Conference on Electrical Machines and Systems, Wuhan, 2008, pp. 3845-3849.

[16] W. N. Fu and L. Li, "Optimal design of magnetic gears with a general pattern of permanent magnet arrangement," IEEE Trans. Appl. Supercond., vol. 26, no. 7, pp. 1-5, 2016.
[17] D. Som, K. Li, J. Kadel, J. Wright, S. Modaresahmadi, J. Z. Bird, and W. William, "Analysis and testing of a coaxial magnetic gearbox with flux concentration halbach rotors," IEEE Trans. Magn., vol. 53, no. 11, pp. 1-6, 2017.
[18] Y. Chen, W. N. Fu, and W. Li, "Performance analysis of a novel triplepermanent-magnet- excited magnetic gear and its design method," IEEE Trans. Magn., vol. 52, no. 7, pp. 1-4, 2016.
[19] Y. Wang, M. Filippini, N. Bianchi and P. Alotto, "A review on magnetic gears: topologies, computational models and design aspects," XIII International Conference on Electrical Machines (ICEM), Alexandroupoli, 2018, pp. 527-533.
[20] K. Li and J. Z. Bird, "A review of the volumetric torque density of rotary magnetic gear designs," 2018 XIII International Conference on Electrical Machines (ICEM), Alexandroupoli, 2018, pp. 2016-2022.
[21] Y. Chen, W. N. Fu, S. L. Ho and H. Liu, "A Quantitative Comparison Analysis of Radial-Flux, Transverse-Flux, and Axial-Flux Magnetic Gears," in IEEE Transactions on Magnetics, vol. 50, no. 11, pp. 1-4, Nov. 2014.
[22] D. J. Evans and Z. Q. Zhu, "Influence of design parameters on magnetic gear's torque capability," 2011 IEEE International Electric Machines & Drives Conference (IEMDC), Niagara Falls, ON, 2011, pp. 1403- 1408.
[23] N. W. Frank and H. A. Toliyat, "Gearing ratios of a magnetic gear for wind turbines," 2009 IEEE International Electric Machines and Drives Conference, Miami, FL, 2009, pp. 1224-1230.
[24] P. B. Reddy, A. M. EL-Refaie, S. Galioto, and J. P. Alexander, "Design of synchronous reluctance motor utilizing dual-phase material for traction applications," IEEE Trans. Ind. Appl., vol. 53, no. 3, pp. 1948-1957, May/Jun. 2017.
[25] A. M. EL-Refaie et al., "Advanced High-Power-Density Interior Permanent Magnet Motor for Traction Applications," in IEEE Transactions on Industry Applications, vol. 50, no. 5, pp. 3235-3248, Sept.-Oct. 2014.